Center for Turbulence Research
Proceedings of the Summer Program 2008

LES of two-phase reacting flows

By M. Sanjosé†, T. Lederlin, L. Gicquel†, B. Cuenot†, H. Pitsch, N. García-Rosa‡, R. Lecourt‡ AND T. Poinsot¶

Large-eddy simulations (LES) of a two-phase flow in an experimental burner are performed using two different solvers, CDP from Stanford and AVBP from CERFACS, on the same grid and for the same operating conditions. The numerical results of both codes are evaluated by comparison of experimental data. The testrig, called MERCATO, is an aeronautical-type swirl-stabilized spray burner, fueled with liquid Jet-A kerosene. The CDP code uses an implicit incompressible gas solver together with a Lagrangian liquid-phase tracking method and a flamelet model for combustion. The AVBP uses an explicit compressible gas solver, a mesoscopic Eulerian approach for the dispersed droplet phase and a thickened flame model for turbulence-combustion interaction. Gas and liquid phases dynamics, droplet dispersion and fuel evaporation and burning are qualitatively and quantitatively evaluated. Results show a good agreement of both methods for the non-reacting but evaporating case. Preliminary results for the flame are also shown and exhibit more important differences.

1. Introduction

Large-eddy simulation (LES) is becoming a standard tool for gaseous reacting flows (Mahesh *et al.* 2004; Selle *et al.* 2004; Moureau *et al.* 2005; Roux *et al.* 2005; Poinsot & Veynante 2005). The application of LES to non-reacting two-phase flows (Apte *et al.* 2003; Riber *et al.* 2006, 2008) or to reacting two-phase flows (Ham *et al.* 2003; Menon & Patel 2006; Patel & Menon 2008; Boileau *et al.* 2008*a*,*b*) is at an earlier stage because of the multiple challenges associated with the description of fuel spray atomization, of interaction of droplets with flames or walls and the lack of experimental results which can be used to validate CFD results. This report presents a joint effort between CERFACS, Stanford, ONERA and IMFT to perform LES of an experimental two-phase combustor installed at ONERA, Toulouse. This configuration has been computed with two different solvers (CDP of Stanford and AVBP of CERFACS) and results have been compared to experimental ONERA results for three Cases: (I) purely gaseous non-reacting flow (II) gaseous non-reacting flow with evaporating droplets and (III) reacting flow with droplets. Available experimental data for Cases I and II include velocity fields for the gas and for the droplets. For Case III (reacting), the velocity field of droplets in the fresh gases has been measured.

The numerical efficiency of solvers used for two-phase flows is an additional constraint which was studied during this work. For single-phase flows, parallel speed-ups of the order of 5000 are not uncommon (www.cerfacs.fr/cfd/parallel.html). Maintaining a similar parallel efficiency for a two-phase flow solver raises additional questions. A first one is the choice of the time-advancement scheme: Using implicit time advancement for LES is an

† CERFACS, CFD team, 42 Av Coriolis, 31057 Toulouse, France
‡ ONERA Toulouse, France
¶ IMF Toulouse, INP de Toulouse and CNRS, 31400 Toulouse, France

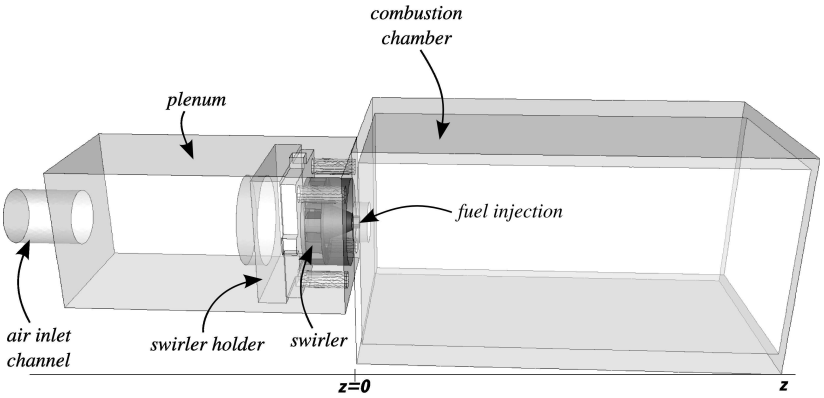

FIGURE 1. The MERCATO configuration (ONERA Toulouse).

obvious path to increase efficiency but developing efficient implicit solvers on thousands of processors is difficult. A second issue is the paradigm chosen to describe the dispersed phase: Both Euler-Lagrange (EL) and Euler-Euler (EE) (Mahesh *et al.* 2006; Riber *et al.* 2008; Boileau *et al.* 2008*b*; Patel & Menon 2008) are found in LES of two-phase flows. The EL method is more commonly used as it allows a straightforward implementation of physical aspects, such as poly-dispersion of a spray, crossing trajectories, wall bouncing of droplets and droplet-wake combustion. However, the EE approach is sometimes preferred for its identical parallelization of liquid and gas solvers. This continuous approach provides naturally converged statistics over the droplets number, contrary to the EL approach which may require longer simulation time for convergence. Here again, precision and scaling possibilities on massively parallel machines are crucial issues. During this work, the influence of time advancement and of dispersed phase treatment was studied by using an implicit Euler-Lagrange solver (CDP) and an explicit Euler-Euler solver (AVBP).

2. Configuration

The experimental rig MERCATO (Fig. 1) is a swirled combustor fed with air and Jet-A liquid fuel. The regimes considered here are presented in Table 1. The flow conditions are different for the reacting and non-reacting Cases. For Case II (non-reacting), the air is heated up to 463 K to enhance evaporation and reduce the formation of liquid fuel films on visualization windows. Case I and Case II are operated at the same air inlet temperature and with the exact geometry displayed in Fig. 1. For these Cases the flow exits in the atmosphere, while for Case III an additional exhaust pipe is added after the combustion chamber.

For Cases I and II, the comparison is performed for the mean and RMS velocity fields of the gas and (for Case II) of the droplets. For Case III, the droplet velocity field and the flame position will be used for comparison. In non-reacting Cases I and II, velocities and size measurements were performed using PDA-LDA. For Case III, droplet velocities are measured using PIV.

Case	Pressure (atm)	Air temperature (K)	Liquid temperature (K)	Air flow rate (g/s)	Fuel flow rate (g/s)	Equivalence ratio
I: gaseous flow	1	463	–	15	–	–
II: gaseous flow + droplets	1	463	300	15	1	1.0
III: reacting two-phase flow	1	285	285	26	2.9	1.6

TABLE 1. Summary of regimes.

3. Description of solvers and models

Numerical methods used in both LES solvers for the gas phase have been extensively described before (Moureau *et al.* 2005; Selle *et al.* 2004; Schmitt *et al.* 2007; Mahesh *et al.* 2004; Ham & Iaccarino 2004; Riber *et al.* 2008) and will only be summarized here.

CDP: Euler / Lagrange method

The LES solver CDP solves implicitly the incompressible Navier-Stokes equations. The time integration of CDP is based on the fractional-step method (Kim & Moin 1985) and the space integration relies on a second-order central scheme which conserves the kinetic energy (Mahesh *et al.* 2004; Ham & Iaccarino 2004). The dynamic Smagorinsky model (Germano *et al.* 1991) is used to model the subgrid stress tensor. Droplet dynamics are simulated using a Lagrangian point-particle model. It is assumed that (1) the density of the droplets is much greater than that of the carrier fluid, (2) the droplets are dispersed and collisions between them are negligible, (3) the droplets are much smaller than the LES filter width, (4) droplet deformation effects are small and (5) motion due to shear is negligible.

AVBP: Euler / Euler method

The AVBP code solves the compressible Navier-Stokes equations with a third-order scheme for spatial differencing and a Runge-Kutta time advancement (Colin & Rudgyard 2000; Moureau *et al.* 2005). The Wale model is used to model SGS tensors (Nicoud & Ducros 1999). Boundary conditions are handled with the NSCBC formulation (Poinsot & Veynante 2005; Poinsot & Lele 1992). The treatment of the dispersed phase is based on a monodisperse Eulerian mesoscopic approach, following the methodology of the non-reacting configuration of Riber *et al.* (2008) and of the reacting cases of Boileau *et al.* (2008*a*,*b*). Conservation equations are solved for droplet number density, liquid volume fraction, droplet mesoscopic velocity components and droplet enthalpy. The present EE method neither takes into account local poly-dispersion nor trajectory crossing of droplets. If two packets of droplets, having different mesoscopic velocity, temperature and mean droplet diameter, intersect, they collapse into one packet having the averaged properties of the preceding two. Multiple Euler-Euler formulations allow to correct these limitations (Laurent *et al.* 2004; Desjardins *et al.* 2006), but the focus of the present work was not to develop this aspect.

Solver Surrogate reference	Composition (in volume)	Molar Weight (g/mol)	Boiling Temperature (K)
CDP-EL (Peters 2006)	80% of n-decane 20% tri-methyl-benzene	165	606.5
AVBP-EE (Luche 2003)	74% of n-decane 15% propyl-benzene 11% propyl-cyclo-hexane	137.2	445.1

TABLE 2. Summary of used surrogate fuel properties.

4. Kerosene description and evaporation models

4.1. *Choice of a surrogate for kerosene*

In the experiments, the injected fuel is a commercial aviation kerosene Jet-A, which is a mixture of a large number of hydrocarbons and additives. In the LES calculations, kerosene is modeled by a single *meta* species built as an average of the thermodynamic properties of kerosene multi-component surrogates. The liquid density for both surrogates is 781 kg/m^3, the heat of vaporization is approximately 2.5×10^5 J/kg, the liquid heat capacity is approximately 2×10^3 J/kg/K. The properties are very close for both surrogate fuels' differences are summarized in Table 2.

4.2. *Evaporation model*

In both solvers, a classical model is employed for evaporation, which assumes infinite thermal conductivity of the liquid: The evaporation rate is driven by the thermal and species diffusion from the droplet surface into the gas phase.

In the AVBP-EE solver, the Nusselt Nu and Sherwood Sh numbers are modified following the Ranz-Marshall correlations (Ranz & Marshall 1952) to take into account the effect of droplet inertia in the carrier phase. In the CDP-EL solver, this effect is modeled by the multiplicative correction for heat and mass transfer proposed by Faeth (1983), Faeth & Lazar (1971).

The liquid/gas interface is assumed to be in thermodynamic equilibrium, the Clausius-Clapeyron equilibrium vapor pressure relationship is used to compute the fuel mass fraction at the droplet surface. To take into account the modification of composition and temperature of the gas around the droplets, the gas properties are evaluated using the *one-third two-thirds* rule (Hubbard *et al.* 1975) for constant reference mass fractions and temperature.

5. Boundary conditions

Both solvers use zero velocity at walls for the gas velocity. In the EL simulation, particles are elastically bouncing at walls while in the EE simulation, the liquid phase follows a slip condition at walls. One of the main factors controlling the dispersion of the droplets is the description of the injection pattern. In this study there is no computation of primary atomization at the injector outlet and both EE and EL approaches have to rely on measurements and empirical correlations to adjust the injection condition on the atomizer outlet plane.

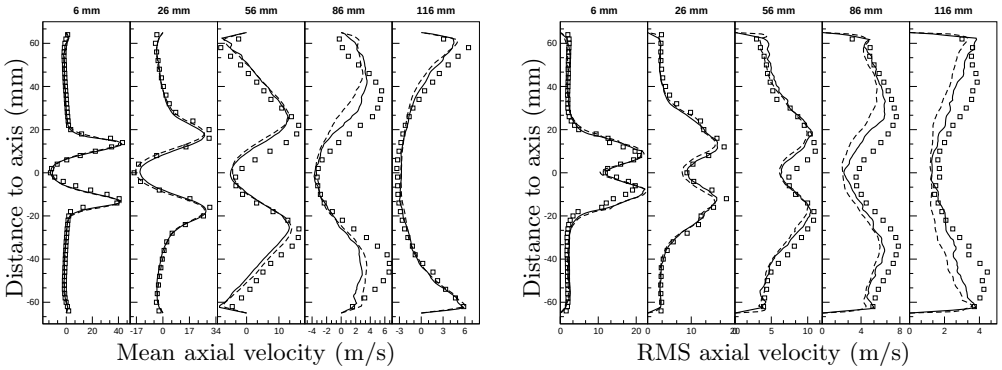

FIGURE 2. Axial velocity (Case I). Left: mean, right: RMS. □ LDA, − CDP-EL, - - AVBP-EE.

The injection boundary conditions are based on a methodology which takes into account radial, tangential and axial outflow velocity components. Following the empirical correlations of Rizk & Lefebvre (1985), inlet profiles are built from the following parameters: the liquid flow rate, the spray angle and the internal geometry of the Simplex atomizer. These inlet profiles are used in the CDP-EL simulation. In the AVBP-EE continuous approach, the discharge orifice of the atomizer (diameter 0.5 mm) must be sufficiently meshed to control the flow rate through the boundary correctly. A compromise between discretizing the boundary patch and keeping a reasonable time step is found in enlarging the boundary condition area which is translated a few millimeters downstream from the real injection position. Boundary profiles are built from the inlet empirical profiles (used in CDP-EL) and applying the air entrainment model of Cossali (2001). For the EL approach in CDP, the initial droplet diameter is sampled from a Rosin-Rammler distribution fitted with the experimental probability density function (pdf) of droplet diameters at the first measurement location ($z = 6$ mm). For the AVBP-EE simulation, the first moment of the distribution is used for the injection.

6. Gas flow without droplets (Case I)

Before considering the dispersion and evaporation and combustion of droplets, it is necessary to evaluate the precision of the computations for the carrier phase: the MERCATO rig was operated without kerosene injection and LDA was performed on the gas phase seeded with fine ($< 2\mu$m) oil droplets so that results can be directly compared to gas-phase simulations of CDP and AVBP. The unstructured mesh used for both codes contains 3.5 Mcells and 650000 nodes.

Figure 2 shows mean and RMS gas velocity profiles in the transverse direction for five axial positions, ranging from $z = 6$ to $z = 116$ mm from the injection plane. AVBP and CDP results are compared to the experimental data (symbols). Both solvers capture the flow correctly, considering that there is no adjustable inlet boundary condition which can be tuned for this flow. The averaging time in both LES codes is of the order of 400 ms corresponding to approximately 10 flow-through times. The time step used for AVBP is 0.22 microseconds (imposed by the acoustic CFL condition), while the time step for CDP is 11 microseconds (corresponding to a convective CFL number of 3).

Some differences between the two codes appearn especially for RMS values (Figs. 2 and 3, right) at locations where both solvers under-predict the RMS levels. CDP predicts

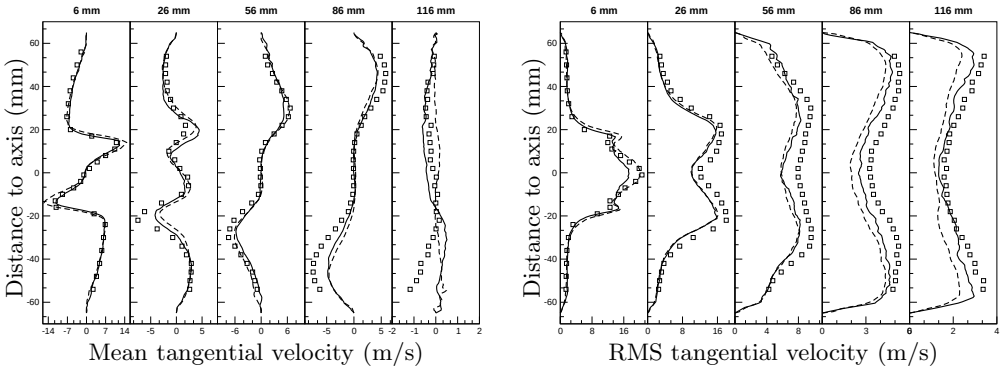

FIGURE 3. Tangential velocity (Case I). Left: mean, right: RMS. □ LDA, − CDP-EL, - - AVBP-EE.

more precise axial velocity RMS levels at the two last comparison stations showing the influence of the kinetic energy conservation by the numerical scheme. Some discrepancies may be observed for the mean tangential velocity (Fig. 3, left) at the two last stations. The experimental profile is actually not symmetric at the last station, pointing out that the measurement error in this low-speed region is large.

For this case, both AVBP and CDP also show that a strong Precessing Vortex Core (spining at 800 Hz) dominates the unsteady activity and the RMS velocity field. This frequency was also evaluated in the experimental spectra of pressure and velocity. Since this is a classical result for such flows (Roux *et al.* 2005; Selle *et al.* 2006), it is not described in greater detail here.

7. Gas flow with evaporating droplets (Case II)

For Case II, droplets are injected starting from a well-established gas-phase solution. Figure. 4 shows an instantaneous view of droplets' distribution in the combustion chamber. Both simulations capture the same structures of droplet preferential concentration: The central recirculation has a low droplet density, dense pockets of droplets can be seen in the shear layer of the swirled air jet and droplets are trapped in the recirculation zone in corners of the chamber. Such droplet concentrations lead to fuel vapor inhomogeneities through the evaporation source terms, as shown in Fig. 5. In the CDP simulation, the liquid seems to evaporate more strongly close to the injector exit, as indicated by the evaporation rate isocontours. This may be due to the evaporation of small droplets from the poly-disperse spray.

The velocity profiles of droplets are compared in Figs. 6 through 9. For these figures, only the averaged velocity (overall droplet size classes) is shown. Since the EE approach used here provides only a mean droplet size, no attempt was made to look at size-conditioned statistics. The averaging time in both LES codes is of the order of 80 ms corresponding to approximately 2 flow-through times. The CDP-EL statistical results shows non-converged quantities in areas where the droplet number density is low, such as the chamber centerline. The EE method takes advantage of its continuous mesoscopic approach (transported quantities are averaged over the particle realizations), and results show smoother profiles. To delay the spray impingement on the visualization windows, the experimentalists have increased the air-flow rate to perform the LDA measurement at $z = 56$ mm. Thus the comparisons at this location must be taken with care.

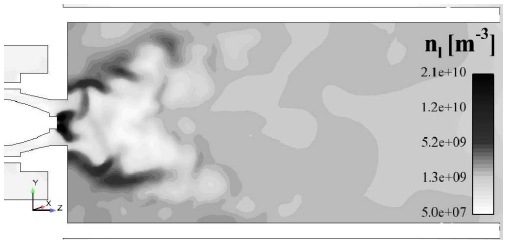

(a) AVBP-EE: droplet number density (grayscale).

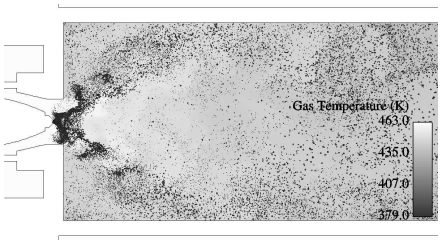

(b) CDP-EL: droplets' position (dots), gas temperature (grayscale).

FIGURE 4. Instantaneous droplets distribution in the MERCATO chamber (Case II).

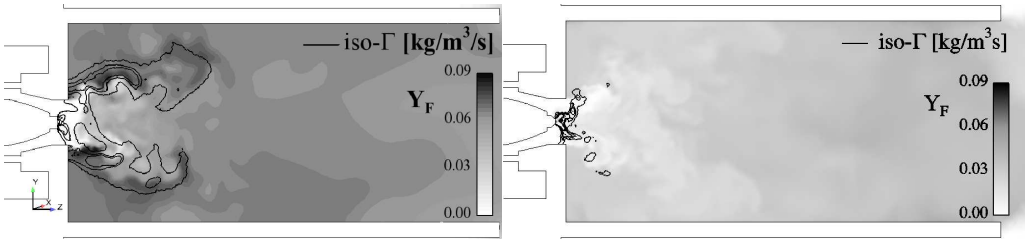

FIGURE 5. Instantaneous kerosene vapor mass fraction (grayscale) and evaporation rate (isocontours). Left: AVBP-EE results, right: CDP-EL results (Case II).

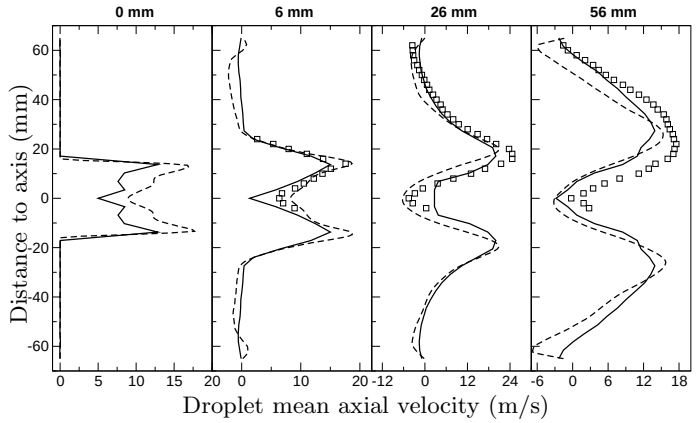

FIGURE 6. Mean axial velocity (Case II). □ LDA, − CDP-EL, - - AVBP-EE.

The agreement between the two LES codes and the experimental profiles is good at $z = 6$ mm for the droplet axial velocity, showing that the injection procedures described in Sec. 5 are suitable for such flows, where two-phase effects and droplet drag are significant. The agreement is still good at $z = 26$ and 56 mm for axial velocity. Looking at the axial RMS values, both simulations fail to reproduce the shape and the levels of RMS at the first location. For the next stations, both codes reproduce the correct fluctuation levels, but the shapes of the profiles are not well-captured, even though the experimental data are quite noisy.

Concerning the mean tangential component shown in Fig. 8, both simulations predict the correct opening of the spray. Results show good agreements at $z = 6$ mm but the

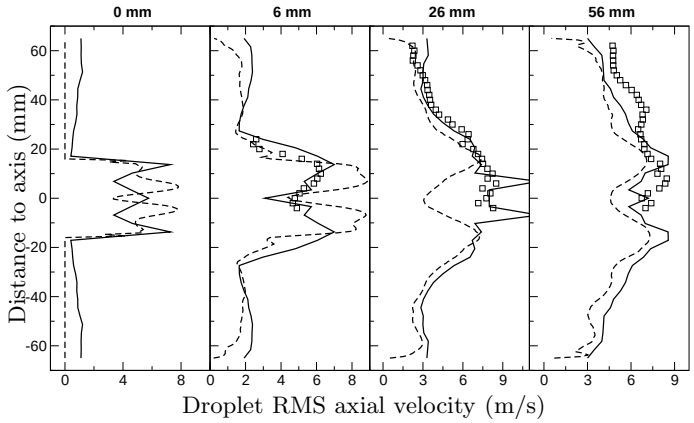

FIGURE 7. RMS axial velocity (Case II). □ LDA, − CDP-EL, - - AVBP-EE.

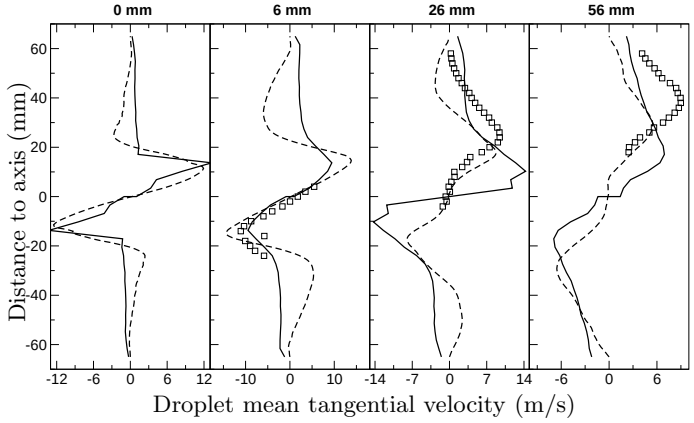

FIGURE 8. Mean tangential velocity (Case II). □ LDA, − CDP-EL, - - AVBP-EE.

discrepancies increase as the spray moves downstream. The maximum value and location are not well-predicted. Looking at the RMS values of the droplet tangential velocity component shown in Fig. 9, the shape and values are very well-reproduced by the AVBP-EE simulation. The CDP-EL statistics of this component are not converged.

More generally, both approaches correctly predict the right spray dynamics and fluctuations and their prediction is comparable. The drawback of the particular EL approach is that the simulation should be performed over a longer physical time than the EE simulation to collect statistically converged data. This convergence time depends both on the gas characteristic time scale and on the liquid mass loading.

Figure 10 shows that the AVBP-EE fails in predicting the droplet diameter distribution, in terms of shapes and values. The CDP-EL results exhibit a better agreement in terms of value, but still the shape of the mean diameter profile is not well-reproduced at $z = 6$ and $z = 26$ mm. Again it must be noted that the experimental profiles are quite noisy, and the CDP-EL are not sufficiently converged to decide on its accuracy.

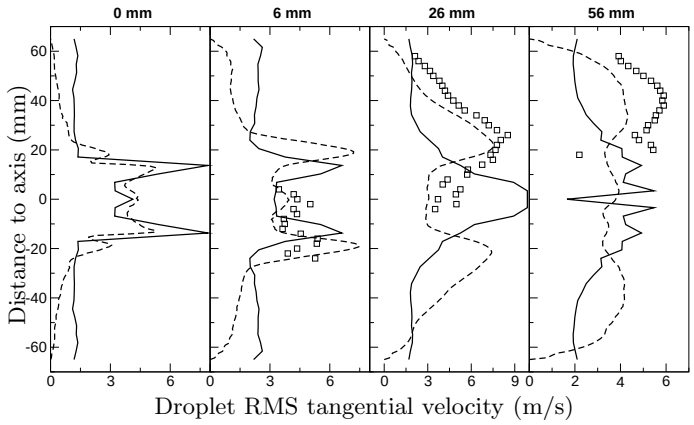

FIGURE 9. RMS tangential velocity (Case II). □ LDA, − CDP-EL, - - AVBP-EE.

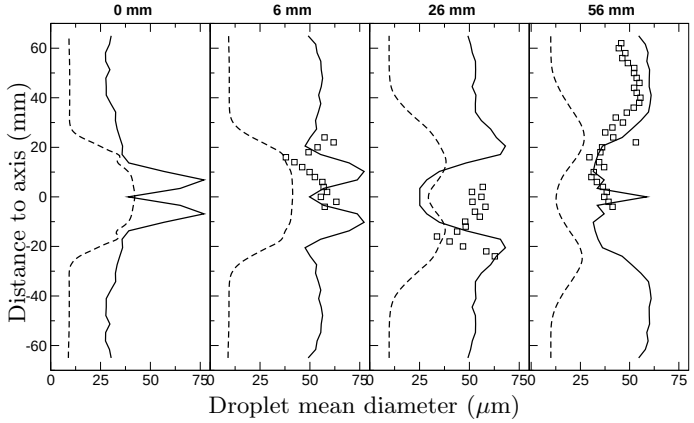

FIGURE 10. Droplet mean diameter (Case II). □ LDA, − CDP-EL, - - AVBP-EE.

8. Reacting two-phase flow (Case III)

The chemical model used in CDP uses a flamelet approach based on a progress variable and a mixture fraction (Pierce & Moin 2004). Chemistry is tabulated from a full chemical scheme. In AVBP the reaction rates of the combustion of the kerosene surrogate are calculated by an Arrhenius law. The chemical scheme is a two-step mechanism, with an adaptation of the pre-exponential factor (Boudier *et al.* 2008), built to fit the laminar flame speed values as a function of local equivalence ratio evaluated with the detailed mechanism of Luche (2003). The interaction between turbulence and combustion is modeled using the DTF (dynamic thickened flame) model (Colin *et al.* 2000).

For this work, reacting flow LES were initialized the same way in both codes: starting from a non-reacting regime, the chamber and exhaust gases were replaced by burnt gases and the heat-release model was subsequently started. Even though this procedure does not correspond to a possible event in the real world, it allows to rapid convergence with a well-established flame.

The flame structure obtained at steady state is complex: the zones where the droplets evaporate overlap the reaction zones and a significant amount of liquid fuel actually crosses the flame front and evaporates within burnt gases leading to very strong gradients

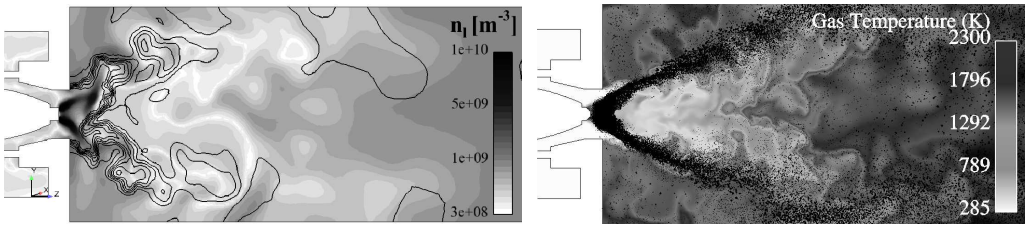

(a) AVBP-EE: droplets density (grayscale) and gas temperature (isocontours).

(b) CDP-EL: droplets position (dots) and gas temperature (grayscale).

FIGURE 11. Instantaneous droplet distribution in the MERCATO chamber (Case III).

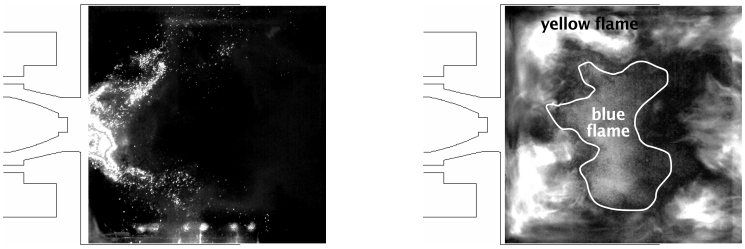

(a) Enlightened droplets on a laser sheet.

(b) Flame structure.

FIGURE 12. High-speed camera visualizations (Case III).

of fuel equivalence ratio and to flame structures which cannot be found in gaseous flames: in the present combustor, diffusion flames are formed betwen oxygen injected in the air stream and fuel evaporated in the burnt gases. This is evidenced in Fig. 11, which displays an instantaneous field of droplet distribution and the temperature distribution in the burner central plane. High kerosene concentrations are found in hot regions near the tip of the flame. At these locations, the local equivalence ratio can reach values close to 2. A partially premixed flame occurs in the central recirculation zone as the droplet number density is lower and hot gases are stabilized.

Since the flame structure appears to be quite different in AVBP and CDP cases (see Fig. 11) and since the available experimental visualizations do not accurately localize the flame front (Fig. 12), a reliable assessment of codes and models can not be made at the present time, preliminary comparisons of chemistry models on simpler kerosene/air flames structures should be performed first. Does the flame attached on the nose of the atomizer as in the CDP field? Is it due to the poly-disperse EL approach or the flamelet combustion model? These questions will be addressed by the authors in future studies.

9. Conclusions

The precision of two LES solvers has been evaluated in the case of a swirled liquid kerosene / air combustor developed at ONERA Toulouse. Even though the two solvers use very different methods, the results obtained for the non-reacting case and for the evaporating non-reacting case agree reasonably and match the experimental results. The reacting case is more difficult and the flame structure is characterized by the fact that evaporation of the liquid kerosene takes place behind or within the flame itself. In the future, when more statistically converged results are available, the comparison will show

whether the flame is located more downstream, as predicted by AVBP, or close to the nozzle, as seen in the CDP results. From these results and further simulations, it will be interesting to analyze if differences in the results arise predominantly from differences in spray and combustion models.

Acknowledgments

The support of Turbomeca and of the French DGA (Délégation Générale de l'Armement) is gratefully acknowledged. Part of this work received funding from the European Community through the project TIMECOP-AE (Project #AST-CT-2006-030828). It reflects only the authors' views and the Community is not liable for any use that may be made of the information contained therein.

REFERENCES

Apte, S. V., Mahesh, K., Moin, P. & Oefelein, J. C. 2003 Large-eddy simulation of swirling particle-laden flows in a coaxial-jet combustor. *Int. J. Multiphase Flow* **29** (8), 1311–1331.

Boileau, M., Pascaud, S., Riber, E., Cuenot, B., Gicquel, L., Poinsot, T. & Cazalens, M. 2008*a* Investigation of two-fluid methods for Large Eddy Simulation of spray combustion in gas turbines. *Flow, Turb. and Combustion* **80** (3), 291–321.

Boileau, M., Staffelbach, G., Cuenot, B., Poinsot, T. & Bérat, C. 2008*b* LES of an ignition sequence in a gas turbine engine. *Combust. Flame* **154** (1-2), 2–22.

Boudier, G., Gicquel, L. Y. M. & Poinsot, T. 2008 Effect of mesh resolution on large eddy simulation of reacting flows in complex geometry combustors. *Combust. Flame* **155** (1-2), 196–214.

Colin, O., Ducros, F., Veynante, D. & Poinsot, T. 2000 A thickened flame model for large eddy simulations of turbulent premixed combustion. *Phys. Fluids* **12** (7), 1843–1863.

Colin, O. & Rudgyard, M. 2000 Development of high-order Taylor-Galerkin schemes for unsteady calculations. *J. Comput. Phys.* **162** (2), 338–371.

Cossali, G. 2001 An integral model for gas entrainment into full cone sprays. *J. Fluid Mech.* **439**, 353–366.

Desjardins, O., Fox, R. O. & Villedieu, P. 2006 A quadrature-based moment closure for the Williams spray equation. In *Proc. of the Summer Program*, pp. 223–234. Center for Turbulence Research, NASA Ames/Stanford Univ.

Faeth, G. M. 1983 Evaporation and combustion of sprays. *Prog. Energy Comb. Sci.* **9**, 1–76.

Faeth, G. M. & Lazar, R. S. 1971 Fuel droplet burning rate in a combustion gas environment. *Am. Inst. Aeronaut. Astronaut. J.* **9** (11), 2165–2171.

Germano, M., Piomelli, U., Moin, P. & Cabot, W. 1991 A dynamic subgrid-scale eddy viscosity model. *Phys. Fluids* **3** (7), 1760–1765.

Ham, F., Apte, S. V., Iaccarino, G., Wu, X., Herrmann, M., Constantinescu, G., Mahesh, K. & Moin, P. 2003 Unstructured LES of reacting multiphase flows in realistic gas turbine combustors. In *Annual Research Briefs*, pp. 139–160. Center for Turbulence Research, NASA Ames/Stanford Univ.

Ham, F. & Iaccarino, G. 2004 Energy conservation in collocated discretization

schemes on unstructured meshes. In *Annual Research Briefs*, pp. 3–14. Center for Turbulence Research, NASA Ames/Stanford Univ.

Hubbard, G. L., Denny, V. E. & Mills, A. F. 1975 Droplet evaporation: effects of transient and variable properties. *Int. J. Heat and Mass Transfer* **18**, 1003–1008.

Kim, J. & Moin, P. 1985 Application of a fractional-step method to incompressible navier-stokes equations. *J. Comput. Phys.* **59** (2), 308–323.

Laurent, F., Massot, M. & Villedieu, P. 2004 Eulerian multi-fluid modeling for the numerical simulation of coalescence in polydisperse dense liquid sprays. *J. Comput. Phys.* **194** (2), 505–543.

Luche, J. 2003 Elaboration of reduced kinetic models of combustion. Application to a kerosene mechanism. PhD thesis, Université d'Orléans, LCSR Orleans.

Mahesh, K., Constantinescu, G., Apte, S., Iaccarino, G., Ham, F. & Moin, P. 2006 Large eddy simulation of reacting turbulent flows in complex geometries. *ASME J. Appl. Mech.* **73** (3), 374–381.

Mahesh, K., Constantinescu, G. & Moin, P. 2004 A numerical method for large-eddy simulation in complex geometries. *J. Comput. Phys.* **197** (1), 215–240.

Menon, S. & Patel, N. 2006 Subgrid modeling for simulation of spray combustion in large scale combustors. *Am. Inst. Aeronaut. Astronaut. J.* **44** (4), 709–723.

Moureau, V., Lartigue, G., Sommerer, Y., Angelberger, C., Colin, O. & Poinsot, T. 2005 High-order methods for DNS and LES of compressible multi-component reacting flows on fixed and moving grids. *J. Comput. Phys.* **202** (2), 710–736.

Nicoud, F. & Ducros, F. 1999 Subgrid-scale stress modelling based on the square of the velocity gradient. *Flow, Turb. and Combustion* **62** (3), 183–200.

Patel, N. & Menon, S. 2008 Simulation of spray–turbulence–flame interactions in a lean direct injection combustor. *Combust. Flame* **153** (1-2), 228–257.

Peters, N. 2006 Private Communications.

Pierce, C. D. & Moin, P. 2004 Progress-variable approach for large eddy simulation of non-premixed turbulent combustion. *J. Fluid Mech.* **504**, 73–97.

Poinsot, T. & Lele, S. 1992 Boundary conditions for direct simulations of compressible viscous flows. *J. Comput. Phys.* **101** (1), 104–129.

Poinsot, T. & Veynante, D. 2005 *Theoretical and numerical combustion.* R.T. Edwards, 2nd edition.

Ranz, W. E. & Marshall, W. R. 1952 Evaporation from drops. *Chem. Eng. Prog.* **48** (4), 173.

Riber, E., García., M., Moureau, V., Pitsch, H., Simonin, O. & Poinsot, T. 2006 Evaluation of numerical strategies for LES of two-phase reacting flows. In *Proc. of the Summer Program*, pp. 197–211. Center for Turbulence Research, NASA Ames/Stanford Univ.

Riber, E., Moureau, V., García., M., Poinsot, T. & Simonin, O. 2008 Evaluation of numerical strategies for Large Eddy Simulation of particulate two-phase recirculating flows. *J. Comput. Phys.* **in Press** (accepted Manuscript).

Rizk, N. & Lefebvre, A. 1985 Internal flow characteristics of simplex atomizer. *J. Prop. Power* **1** (3), 193–199.

Roux, S., Lartigue, G., Poinsot, T., Meier, U. & Bérat, C. 2005 Studies of mean and unsteady flow in a swirled combustor using experiments, acoustic analysis and large eddy simulations. *Combust. Flame* **141**, 40–54.

Schmitt, P., Poinsot, T. J., Schuermans, B. & Geigle, K. 2007 Large-eddy simulation and experimental study of heat transfer, nitric oxide emissions and combustion instability in a swirled turbulent high pressure burner. *J. Fluid Mech.* **570**, 17–46.

Selle, L., Benoit, L., Poinsot, T., Nicoud, F. & Krebs, W. 2006 Joint use of compressible Large-Eddy Simulation and Helmoltz solvers for the analysis of rotating modes in an industrial swirled burner. *Combust. Flame* **145** (1-2), 194–205.

Selle, L., Lartigue, G., Poinsot, T., Koch, R., Schildmacher, K.-U., Krebs, W., Prade, B., Kaufmann, P. & Veynante, D. 2004 Compressible large-eddy simulation of turbulent combustion in complex geometry on unstructured meshes. *Combust. Flame* **137** (4), 489–505.